# Picosecond time resolved opto-acoustic imaging with 48 MHz frequency resolution

Allaoua Abbas, Yannick Guillet, Jean-Michel Rampnoux, Pierre Rigail, Eric Mottay, Bertrand Audoin, Stefan Dilhaire

# Picosecond time resolved opto-acoustic imaging with 48 MHz frequency resolution

**A. Abbas,**[1,2,3] **Y. Guillet,**[1,*] **J.-M. Rampnoux,**[2] **P. Rigail,**[3] **E. Mottay,**[3] **B. Audoin,**[1] **and S. Dilhaire**[2]

[1]*Univ. Bordeaux, I2M, UMR 5295, F-33405 Talence, France*
[2]*Univ. Bordeaux, LOMA, UMR 5798, F-33405 Talence, France*
[3]*Amplitude Systèmes, Cité de la Photonique, 11 av de Canteranne, F-33600 Pessac, France*
[*]*yannick.guillet@u-bordeaux.fr*

**Abstract:** A compact femtosecond dual-oscillator pump-probe setup with 48 MHz-repetition rate, relying on asynchronous optical sampling, is presented. The relative timing jitter between both lasers over the whole pump-probe delay range is of the order of or lower than 500 fs. We demonstrate that both a picosecond temporal resolution and a 48 MHz spectral resolution combined with the fast acquisition rate inherent to the asynchronous optical sampling allow performing broadband opto-acoustic imaging with a spectrum covering more than two decades from 300 MHz to 150 GHz. As an illustration, the opto-acoustic response of a supported thin film is investigated, revealing high frequency acoustic echoes close to the epicenter as well as low GHz surface acoustic waves propagating up to 40 $\mu$m away from the epicenter. Semi-analytical calculations have been carried out and perfectly reproduce the dispersion of the surface acoustic waves experimentally observed.



**OCIS codes:** (100.0118) Imaging ultrafast phenomena; (300.6500) Spectroscopy, time-resolved; (300.6320) Spectroscopy, high-resolution.

## References and links

1. C. Thomsen, J. Strait, Z. Vardeny, H. J. Maris, J. Tauc, and J. J. Hauser, "Coherent phonon generation and detection by picosecond light pulses," Phys. Rev. Lett. **53**, 989–992 (1984).
2. C. Thomsen, H. T. Grahn, H. J. Maris, and J. Tauc, "Surface generation and detection of phonons by picosecond light pulses," Phys. Rev. B **34**, 4129–4138 (1986).
3. A. Bartels, F. Hudert, C. Janke, T. Dekorsy, and K. Kohler, "Femtosecond time-resolved optical pump-probe spectroscopy at kilohertz-scan-rates over nanosecond-time-delays without mechanical delay line," Appl. Phys. Lett. **88**, 041117 (2006).
4. P. A. Elzinga, R. J. Kneisler, F. E. Lytle, Ya. Jiang, G. B. King, and N. M. Laurendeau, "Pump/probe method for fast analysis of visible spectral signatures utilizing asynchronous optical sampling," Appl. Opt. **26**, 4303–4309 (1987).
5. A. Schliesser, N. Picque, and T. W. Hansch, "Mid-infrared frequency combs," Nat. Photonics **6**, 440–449 (2012).
6. T. Yasui, E. Saneyoshi, and T. Araki, "Asynchronous optical sampling terahertz time-domain spectroscopy for ultrahigh spectral resolution and rapid data acquisition," Appl. Phys. Lett. **87**, 061101 (2005).
7. G. Klatt, R. Gebs, H. Schäfer, M. Nagel, C. Janke, A. Bartels, and T. Dekorsy, "High-resolution terahertz spectrometer," IEEE J. Sel. Top. Quantum Electron. **17**, 159–168 (2011).
8. T. Yasui, K. Kawamoto, Y. D. Hsieh, Y. Sakaguchi, M. Jewariya, H. Inaba, K. Minoshima, F. Hindle, and T. Araki, "Enhancement of spectral resolution and accuracy in asynchronous-optical-sampling terahertz time-domain spectroscopy for low-pressure gas-phase analysis," Opt. Express **20**, 15071–15078 (2012).

#205233 - $15.00 USD Received 21 Jan 2014; revised 13 Mar 2014; accepted 16 Mar 2014; published 27 Mar 2014

9. G. Pernot, M. Stoffel, I. Savic, F. Pezzoli, P. Chen, G. Savelli, A. Jacquot, J. Schumann, U. Denker, I. MÖnch, C. Deneke, O. G. Schmidt, J. M. Rampnoux, S. Wang, M. Plissonnier, A. Rastelli, S. Dilhaire, and N. Mingo, "Precise control of thermal conductivity at the nanoscale through individual phonon-scattering barriers," Nat. Mater. **9**, 491–495 (2010).
10. S. Dilhaire, G. Pernot, G. Calbris, J. M. Rampnoux, and S. Grauby, "Heterodyne picosecond thermoreflectance applied to nanoscale thermal metrology," J. Appl. Phys. **110**, 114314 (2011).
11. J. Cuffe, O. Ristow, E. Chvez, A. Shchepetov, P. O. Chapuis, F. Alzina, M. Hettich, M. Prunnila, J. Ahopelto, T. Dekorsy, and C. M. Sotomayor Torres, "Lifetimes of confined acoustic phonons in ultrathin silicon membranes," Phys. Rev. Lett. **110**, 095503 (2013).
12. C. Janke, M. Först, M. Nagel, H. Kurz, and A. Bartels, "Asynchronous optical sampling for high-speed characterization of integrated resonant terahertz sensors," Opt. Lett. **30**, 1405–1407 (2005).
13. A. Bartels, R. Cerna, C. Kistner, A. Thoma, F. Hudert, C. Janke, and T. Dekorsy, "Ultrafast time-domain spectroscopy based on high-speed asynchronous optical sampling," Rev. Sci. Instrum. **78**, 035107 (2007).
14. A. Bruchhausen, J. Lloyd-Hughes, M. Hettich, R. Gebs, M. Grossmann, O. Ristow, A. Bartels, M. Fischer, M. Beck, G. Scalari, J. Faist, A. Rudra, P. Gallo, E. Kapon, and T. Dekorsy, "Investigation of coherent acoustic phonons in terahertz quantum cascade laser structures using femtosecond pump-probe spectroscopy," J. Appl. Phys. **112**, 033517 (2012).
15. R. Gebs, G. Klatt, C. Janke, T. Dekorsy, and A. Bartels, "High-speed asynchronous optical sampling with sub-50fs time resolution," Opt. Express **18**, 5974–5983 (2010).
16. A. Bruchhausen, R. Gebs, F. Hudert, D. Issenmann, G. Klatt, A. Bartels, O. Schecker, R. Waitz, A. Erbe, E. Scheer, J. R. Huntzinger, A. Mlayah, and T. Dekorsy, "Subharmonic resonant optical excitation of confined acoustic modes in a free-standing semiconductor membrane at ghz frequencies with a high-repetition-rate femtosecond laser," Phys. Rev. Lett. **106**, 077401 (2011).
17. M. E. Siemens, Q. Li, M. M. Murnane, H. C. Kapteyn, R. Yang, E. H. Anderson, and K. A. Nelson, "High-frequency surface acoustic wave propagation in nanostructures characterized by coherent extreme ultraviolet beams," Appl. Phys. Lett. **94**, 093103 (2009).
18. M. Schubert, M. Grossmann, O. Ristow, M. Hettich, A. Bruchhausen, E. C. S. Barretto, E. Scheer, V. Gusev, and T. Dekorsy, "Spatial-temporally resolved high-frequency surface acoustic waves on silicon investigated by femtosecond spectroscopy," Appl. Phys. Lett. **101**, 013108 (2012).
19. C. Giannetti, B. Revaz, F. Banfi, M. Montagnese, G. Ferrini, F. Cilento, S. Maccalli, P. Vavassori, G. Oliviero, E. Bontempi, L. E. Depero, V. Metlushko, and F. Parmigiani, "Thermomechanical behavior of surface acoustic waves in ordered arrays of nanodisks studied by near-infrared pump-probe diffraction experiments," Phys. Rev. B. **76**, 125413 (2007).
20. V. E. Gusev and A. A. Karabutov. *Laser Optoacoustics* (AIP, New York, 1993).
21. Y. Sugawara, O. B. Wright, O. Matsuda, M. Takigahira, Y. Tanaka, S. Tamura, and V. E. Gusev, "Watching ripples on crystals," Phys. Rev. Lett. **88**, 185504 (2002).
22. T. Fujikura, O. Matsuda, D. M. Profunser, O. B. Wright, J. Masson, ans S. Ballandras, "Real-time imaging of acoustic waves on a bulk acoustic resonator," Appl. Phys. Lett. **93**, 261101 (2008).
23. A. A. Maznev, and A. G. Every, "Surface acoustic waves with negative group velocity in a thin film structure on silicon," Appl. Phys. Lett. **95**, 011903 (2009).
24. B. Bonello, L. Belliard, J. Pierre, J. O. Vasseur, B. Perrin, and O. Boyko, "Negative refraction of surface acoustic waves in the subgigahertz range," Phys. Rev. B **82**, 104109 (2010).
25. W. Li, S. D. Sharples, R. J. Smith, M. Clark, and M. G. Somekh, "Determination of crystallographic orientation of large grain metals with surface acoustic waves," J. Acoust. Soc. Am. **132**, 738–745 (2012).
26. R. K. Shelton, S. M. Foreman, L. S. Ma, J. L. Hall, H. C. Kapteyn, M. M. Murnane, M. Notcutt, and J. Ye, "Subfemtosecond timing jitter between two independent, actively synchronized, mode-locked lasers," Opt. Lett. **27**, 312–314 (2002).
27. T. I. Ferreiro, J. Sun, and D. T. Reid, "Frequency stability of a femtosecond optical parametric oscillator frequency comb," Opt. Express **19**, 24159–24164 (2011).
28. Z. Zhang, C. Gu, J. Sun, C. Wang, T. Gardiner, and D. T. Reid, "Asynchronous midinfrared ultrafast optical parametric oscillator for dual-comb spectroscopy," Opt. Lett. **37**, 187–189 (2012).
29. V. A. Stoica, Y. M. Sheu, D. A. Reis, and R. Clarke, "Wideband detection of transient solid-state dynamics using ultrafast fiber lasers and asynchronous optical sampling," Opt. Express **16**, 2322–2335 (2008).
30. L. Thevenard, E. Peronne, C. Gourdon, C. Testelin, M. Cubukcu, E. Charron, S. Vincent, A. Lemaitre, and B. Perrin, "Effect of picosecond strain pulses on thin layers of the ferromagnetic semiconductor (Ga,Mn)(As,P)," Phys. Rev. B **82**, 104422 (2010).
31. M. Hettich, K. Jacob, O. Ristow, C. He, J. Mayer, M. Schubert, V. Gusev, A. Bruchhausen, and T. Dekorsy, "Imaging of a patterned and buried molecular layer by coherent acoustic phonon spectroscopy," Appl. Phys. Lett. **101**, 191606 (2012).
32. Y. Sugawara, O. B. Wright, and O. Matsuda, "Real-time imaging of surface acoustic waves in thin films and microstructures on opaque substrates (invited)," Rev. Sci. Instrum. **74**, 519–522 (2003).
33. T. Saito, O. Matsuda, M. Tomoda, and O. B. Wright, "Imaging gigahertz surface acoustic waves through the

#205233 - $15.00 USD Received 21 Jan 2014; revised 13 Mar 2014; accepted 16 Mar 2014; published 27 Mar 2014

photoelastic effect," J. Opt. Soc. Am. B **27**, 2632–2638 (2010).
34. T. A. Kelf, W. Hoshii, P. H. Otsuka, H. Sakuma, I. A. Veres, R. M. Cole, S. Mahajan, J. J. Baumberg, M. Tomoda, O. Matsuda, and O. B. Wright, "Mapping gigahertz vibrations in a plasmonic-phononic crystal," New J. Phys. **15**, 023013 (2013).
35. N. Deguil, E. Mottay, F. Salin, P. Legros, and D. Choquet, "Novel diode-pumped infrared tunable laser system for multi-photon microscopy," Microsc. Res. Tech. **63**, 23–26 (2004).
36. S. Dilhaire, J. M. Rampnoux, W. Claeys, and C. Rossignol, "Optical heterodyne sampling device," Patent WO2006FR02384 20061020, FR20050010776 20051021 (2005).
37. L. A. Jiang, S. T. Wong, M. E. Grein, E. P. Ippen, and H. A. Haus, "Measuring timing jitter with optical cross correlations," IEEE J. Quantum Electron. **38**, 1047–1052 (2002).
38. J. E. Rothenberg, "Observation of the transient expansion of heated surfaces by picosecond photothermal deflection spectroscopy," Opt. Lett. **13**, 713–715 (1988).
39. O. B. Wright and K. Kawashima, "Coherent phonon detection from ultrafast surface vibrations," Phys. Rev. Lett. **69**, 1668–1671 (1992).
40. R. Salenbien, R. Cote, J. Goossens, P. Limaye, R. Labie, and C. Glorieux, "Laser-based surface acoustic wave dispersion spectroscopy for extraction of thicknesses, depth, and elastic parameters of a subsurface layer: Feasibility study on intermetallic layer structure in integrated circuit solder joint," J. Appl. Phys. **109**, 093104 (2011).
41. J. Higuet, T. Valier-Brasier, T. Dehoux, and B. Audoin, "Beam distortion detection and deflectometry measurements of gigahertz surface acoustic waves," Rev. Sci. Instrum. **82**, 114905 (2011).
42. T. W. Murray, S. Krishnaswamy, and J. D. Achenbach, "Laser generation of ultrasound in films and coatings," Appl. Phys. Lett. **74**, 3561–3563 (1999).
43. F. H. Featherston and J. R. Neighbours, "Elastic Constants of Tantalum, Tungsten, and Molybdenum," Phys. Rev. **130**, 1324–1333 (1963).
44. T. Dehoux, N. Chigarev, C. Rossignol, and B. Audoin, "Effect of lateral electronic diffusion on acoustic diffraction in picosecond ultrasonics," Phys. Rev. B **77**, 214307 (2008).
45. T. Valier-Brasier, T. Dehoux, and B. Audoin, "Scaled behavior of interface waves at an imperfect solid-solid interface," J. Appl. Phys. **112**, 024904 (2012).
46. L. M. Brekhovskikh, *Waves in layered media* (Academic Press, New York, 1960).
47. I. Tolstoy and E. Usdin, "Wave propagation in elastic plates: Low and high mode dispersion," J. Acoust. Soc. Am. **29**, 37–42 (1957).

## 1. Introduction

The understanding and control of elastic properties of matter at a nanometer scale as well as the investigation of the vibrational landscape of nanostructures in the GHz to THz range has considerably made progress since the emergence of the picosecond opto-acoustics in the mid 80's [1, 2]. In its original form, this experimental method relies on a conventional femtosecond pump-probe setup in a transient reflectivity configuration. Pump and probe pulses are delivered by the same laser and the probe pulse is time delayed with respect to the pump pulse by using moving mirrors mounted on a motorized translation stage. This mechanical motion shows several intrinsic drawbacks, such as fluctuation of the beam pointing, modification of the size of the focal spot on the sample and long acquisition times for pump-probe delays ranging over several nanoseconds [3]. To circumvent these drawbacks, Elzinga *et al.* have introduced asynchronous optical sampling (ASOPS) in 1987 [4]. In this scheme, the moving mirrors are no more necessary and the pump-probe delay is generated by using two pulsed lasers at slightly different repetition rates. The use of the ASOPS technique led to fundamental breakthrough in Fourier transform dual-comb spectroscopy [5], THz time-domain spectroscopy [6–8], nanoscale thermal transport [9–11].

The combined use of ASOPS with picosecond acoustics has emerged from the development of the dual-GHz femtosecond oscillator initiated by Janke et al. [3, 12, 13]. This high repetition rate is ideally suited for investigating the propagation of coherent acoustic phonons with frequencies ranging from few tens of GHz [14] to several THz [15]. In the case of confined acoustic phonons with long lifetimes, the intrinsic spectral resolution imposed by the laser repetition rate can be overcome with a subharmonic resonant optical excitation [16]. However, the downside of such ASOPS setups with high repetition rates is that they do not offer a sufficient spectral resolution to investigate the propagation of low GHz coherent acoustic phonons. For

#205233 - $15.00 USD Received 21 Jan 2014; revised 13 Mar 2014; accepted 16 Mar 2014; published 27 Mar 2014

instance, although high frequency surface acoustic waves (SAWs) have been generated by using one dimensional [17, 18] or two dimensional [19] metallic lithographed arrays, the spectrum of SAWs generated through the optical absorption of a focused laser pulse is in general limited by the optical diffraction limit. Within such limitation, this spectrum ranges from few hundreds of MHz to few GHz [20–25]. Up to now, in the picosecond acoustics field, ASOPS pump-probe setups with low repetition rate lasers [6, 8, 26–28] have taken benefit from the high temporal resolution of the system for investigating the propagation of sub-THz acoustic phonons [29,30].

Another advantage of ASOPS setups is the drastic reduction of acquisition times. Hettich *et al*. have taken benefit of this high acquisition rate to perform time-resolved opto-acoustic imaging over a narrowband acoustic spectrum centered around 80 GHz [31], as it can also be achieved with conventional pump-probe setups [21, 24, 32–34]. However, the combination of both high spectral and high temporal resolutions has not yet been exploited to image the propagation of coherent acoustic phonons.

In this article we present an ASOPS-based setup with repetition rates close to 48 MHz and we demonstrate that this system is ideally suited to perform broadband opto-acoustic imaging with a 1 ps-temporal resolution and a 48 MHz-spectral resolution. In the first part, we describe the structure of the dual-oscillator and we quantify the temporal resolution of the ASOPS pump-probe setup. The latter is in part imposed by the relative timing jitter between both femtosecond laser combs which turns out to be of the order of or lower than 500 fs over the whole pump-probe delay range. In the second part, the ability of this setup to perform broadband opto-acoustic imaging with acoustic spectrum covering more than two decades is illustrated by investigating the propagation of the acoustic waves generated by an opto-acoustic point source located at the free surface of a supported thin film. The upper part of the spectrum, up to 150 GHz, corresponds to bulk acoustic waves (BAWs) propagating back and forth inside the thin film and allows to accurately deduce the thin film thickness. In the lower part of the spectrum, close to 1 GHz, two surface acoustic waves (SAWs) are detected, namely a surface skimming longitudinal wave (SSLW) and a pseudo Rayleigh wave (PRW). The strong dispersion of the low frequency PRW is then analyzed by carrying out semi-analytical calculations. The film thickness is a key parameter for these calculations and it has been measured from the high frequency acoustic echoes. An excellent agreement between experimental and calculated results is demonstrated. The 48-MHz spectral resolution allows to illustrate the dispersion of the PRW in the spectral domain by analyzing the frequency dependence of the group velocity in the 0.3 - 1.2 GHz range.

## 2. ASOPS pump-probe setup

### *2.1. Structure of the dual-oscillator*

The laser source is a compact dual-oscillator (t-Pulse Duo, Amplitudes Systèmes, France) [35]. This system contains two diode-pumped passively mode-locked Yb:KYW laser cavities. The two cavities are located on the same temperature-regulated breadboard. A schematic of the dual-oscillator structure is given in Fig. 1. The asynchronous optical sampling consists in synchronizing the repetition rate of a slave laser (laser #2) at a slightly different value compared with the repetition rate of the master laser (laser #1). In the present dual-oscillator system, the master laser delivers 1.0 W average power, 330 fs pulses at 1027 nm and at a repetition rate $f_{\mathrm{rep},1}$. The slave laser delivers 0.6 W average power, 430 fs pulses at 1040 nm and at a repetition rate $f_{\mathrm{rep},2}$. The repetition rate of each laser is approximately 48 MHz. The beating frequency $\Delta f$ between the two lasers is generated by a frequency synthesizer and is stabilized using an active feedback [36]. Two fast photodiodes PD1 and PD2, followed by low-pass filters (LPF), monitor the fundamental repetition rate of each laser. The electronic signal at $f_{\mathrm{rep},1}$ delivered by PD1 is upshifted by the frequency synthesizer at a slightly higher value $f_{\mathrm{rep},1}+\Delta f$, where $\Delta f = 500\,\mathrm{Hz}$.

#205233 - $15.00 USD Received 21 Jan 2014; revised 13 Mar 2014; accepted 16 Mar 2014; published 27 Mar 2014

A phase detector compares $f_{rep,2}$ and $f_{rep,1}+\Delta f$. One of the cavity mirrors of the slave laser is mounted on a piezoelectric transducer (PZT). The amplified output of the phase detector drives the control voltage of the PZT. The slave cavity length is controlled by the PZT voltage and is adjusted to fulfill the condition $f_{rep,2} = f_{rep,1}+\Delta f$. In the following, the slave (resp. the master) laser will be used as the pump (resp. the probe) laser.

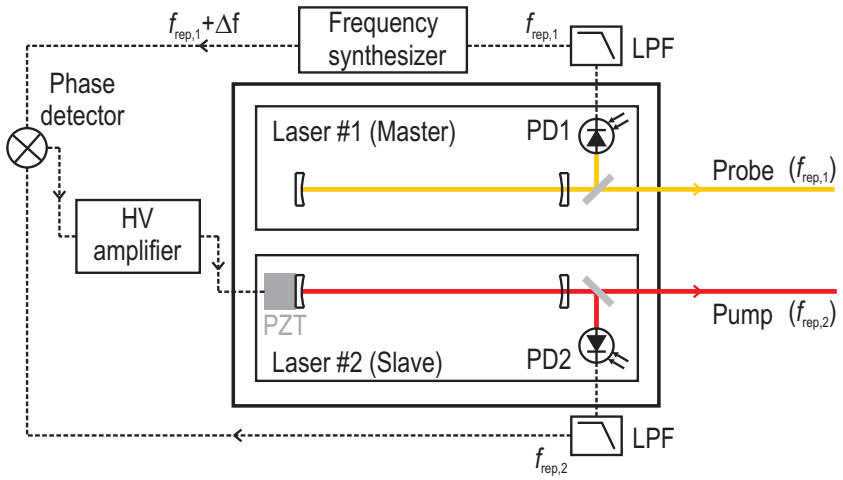


Fig. 1. Simplified scheme of the dual-oscillator system. The fast photodiode PD1 (resp. PD2), associated to the low-pass filter LPF1 (resp. LPF2), monitors the fundamental repetition rate $f_{rep,1}$ (resp. $f_{rep,2}$) of the master laser (resp. slave laser). The frequency synthesizer generates an up-shifted frequency $f_{rep,1}+\Delta f$. The amplified phase detector output controls the piezoelectric transducer (PZT) voltage to adjust the slave cavity length in order to fulfill the condition $f_{rep,2} = f_{rep,1}+\Delta f$.

### 2.2. *Temporal resolution*

The time resolution $\Delta\tau$ of the asynchronous pump-probe setup is imposed by four independent factors [10, 13]: (i) the pump-probe delay increment $\Delta\tau_i = \Delta f/(f_{rep,1}\times f_{rep,2})$ generated by the beating frequency $\Delta f$, (ii) the integrated response of several probe pulses over $\Delta\tau_d = f/(B\times f_{rep,2})$ since the detector bandwidth $B$ is lower than the lasers repetition rate, (iii) the laser pulses duration $\Delta\tau_1$ and $\Delta\tau_2$ and (iv) the relative timing jitter $\Delta\tau_j$ between the two synchronized lasers.

With $\Delta f = 500\,\text{Hz}$ and $f_{rep,1}\approx f_{rep,2}\approx 48\,\text{MHz}$, $\Delta\tau_i$ is measured at 225 fs. The detector bandwidth of $B = 15\,\text{MHz}$ leads to $\Delta\tau_d = 700\,\text{fs}$. The pulses duration $\Delta\tau_1$ and $\Delta\tau_2$ and the jitter $\Delta\tau_j$ are measured with a home-built all-optical correlator presented in Fig. 2. In order to measure temporal duration of the pulses, each laser is first injected separately and its auto-correlation is recorded. Assuming a squared-hyperbolic secant temporal profile, probe and pump pulses durations are measured at $\Delta\tau_1 = 430\,\text{fs}$ and $\Delta\tau_2 = 330\,\text{fs}$, respectively. The relative timing jitter characterization is then performed by injecting the two lasers simultaneously in the correlator and by acquiring the resulting cross-correlation between pump and probe pulses. This acquisition scheme relies on the idea developed by Gebs *et al.* [15]. The optical path difference $\Delta L$ selects the pump-probe delay at which the jitter is measured. In order to cover the whole pump-probe delays offered by the lasers repetition rate, i.e. from 0 to 21 ns, $\Delta L$ has to be adjustable from 0 to 6.3 meters.

Figure 3 shows the relative timing jitter for $\Delta f = 500\,\text{Hz}$ and for pump-probe delays ranging from 0 to 21 ns. The jitter increases with respect to the pump-probe delay, as expected for

#205233 - $15.00 USD Received 21 Jan 2014; revised 13 Mar 2014; accepted 16 Mar 2014; published 27 Mar 2014

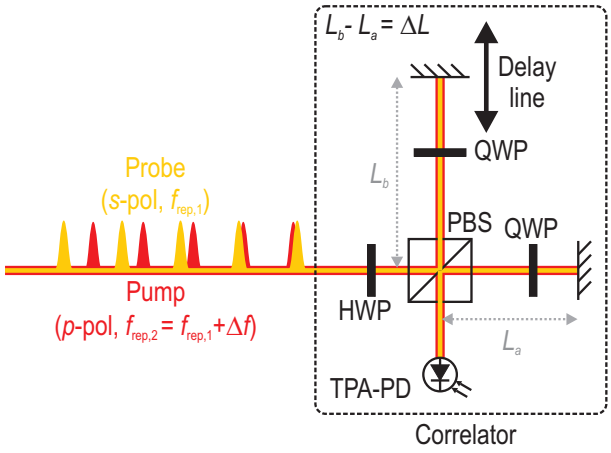


Fig. 2. Scheme of the correlator used for measurements of the pulses duration and of the relative timing jitter. The half-wave plate (HWP) and the polarizing beamsplitter (PBS) allow to inject half of the power of the two orthogonally polarized lasers (*p*-polarized pump pulses and *s*-polarized probe pulses) in each arm of the correlator. The optical path difference $L_a - L_b$ between both arms is denoted $\Delta L$ and is controlled by a retroreflector mounted on a motorized translation stage. After two passages through the quarter-wave plates (QWP), each beam has its polarization 90°-rotated and is directed towards a GaAsP two-photon absorption photodiode (TPA-PD). Photons energy (1.20 eV) is below the 1.83 eV-gap of GaAsP. This photodiode thus generates a transient electric signal each time it absorbs simultaneously two pulses.

passively mode-locked lasers [37]. It is worthwhile noting that, in spite of this cumulative effect, the jitter $\Delta\tau_j$ is of the order of or lower than 500 fs even for delay as large as 21 ns. This value is close to the jitter reported by Yasui *et al.* with two synchronized 50.5 MHz mode-locked femtosecond lasers [8]. The overall time resolution $\Delta\tau$ in the pump-probe experiments presented in the following is given by the quadratic sum of $\Delta\tau_1$, $\Delta\tau_2$, $\Delta\tau_j$, $\Delta\tau_i$ and $\Delta\tau_d$. $\Delta\tau$ is therefore of the order of 1 ps.

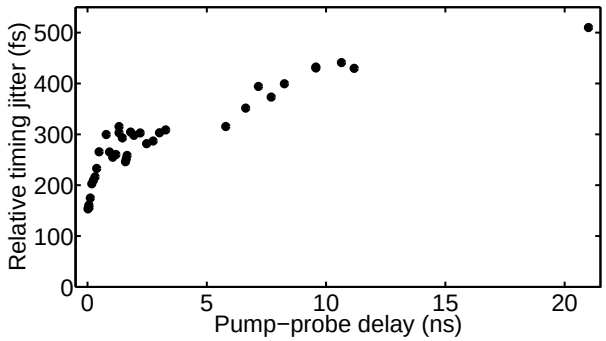


Fig. 3. Measured relative timing jitter between pump and probe pulses versus pump-probe delay for $\Delta f = 500$ Hz.

#205233 - $15.00 USD Received 21 Jan 2014; revised 13 Mar 2014; accepted 16 Mar 2014; published 27 Mar 2014

## 3. Broadband and high spectral resolution opto-acoustic imaging

### *3.1. Asynchronous pump-probe opto-acoustic imaging setup*

The time-resolved opto-acoustic imaging setup relies on the pump-probe scheme in a transient reflectivity configuration presented in Fig. 4(a). All the results presented hereinafter have been obtained for a beating frequency $\Delta f = 500\,\text{Hz}$. The two lasers are recombined by the beamsplitter BS4 and focused on the sample through a $\times 50$ microscope objective. The reflected probe beam is directed with the beamsplitter BS5 towards a amplified silicon photodiode (PD). Pump and probe pulse durations are 430 fs and 330 fs, respectively: these durations are sufficiently long to neglect the temporal broadening induced by the dispersion of the different optical elements throughout the setup. A part of each laser is picked off (BS1 and BS2), recombined (BS3) and focused through a $\times 10$ microscope objective on a GaAsP two-photon absorption photodiode (TPA-PD). The TPA-PD signal is amplified by a custom-built preamplifier. At repeated times delayed of the beating period $1/\Delta f$, the transient electric signal delivered by the TPA-PD is used as a trigger signal for the transient reflectivity acquisition. To perform a two dimensional scan, the pump-probe distance at the surface of the sample is controlled with an afocal telescope lens pair (L1 and L2, $f = 100\,\text{mm}$ focal lengths) inserted in the pump beam before the beamsplitter BS4. The lens L2 is fixed and the lens L1 is mounted on a motorized *xy*-stage. This controlled translation of L1 imposes the incident angle of the collimated pump beam on the entrance pupil of the microscope objective and thus controls the pump-probe distance on the sample surface. By varying this angle, a two dimensional scan over a $100\,\mu\text{m} \times 100\,\mu\text{m}$ area can be performed. At each pixel of the image, the transient reflectivity is recorded over 21 ns with a subpicosecond temporal step. The acquisition time of the pump-probe signal for each pixel varies from few seconds to few tens of seconds, depending on the signal-to-noise ratio of the measurements. In other words, the strength of the ASOPS rests in its ability to acquire several thousands of temporally resolved images of the transient reflectivity. This inherent consequence of the ASOPS turns out to be one of the main advantages compared to conventional methods implying the use of a mechanical delay line [21, 24].

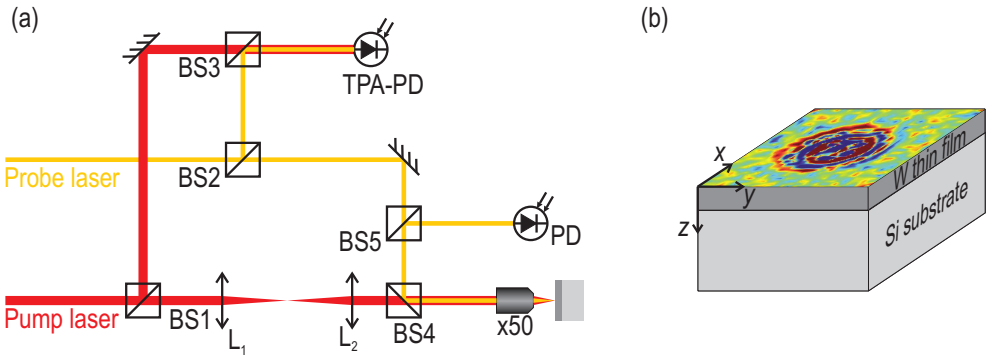


Fig. 4. (a) Asynchronous pump-probe opto-acoustic imaging setup. The transient signal generated on the TPA-PD is used as a trigger signal for the transient reflectivity acquisition. BS: beamsplitter, PD: amplified silicon photodiode. (b) Structure of the sample studied: an opto-acoustic point source is generated at the free surface of a thin tungsten layer supported by a (100)-silicon substrate.

#205233 - $15.00 USD Received 21 Jan 2014; revised 13 Mar 2014; accepted 16 Mar 2014; published 27 Mar 2014

### 3.2. Opto-acoustic response of a supported thin film

The sample under investigation is depicted in Fig. 4(b). A thin tungsten layer is deposited on top of a (100)-silicon substrate. The pump pulse is focused on the free surface of the film. The energy of the pump pulse at the sample position is 0.5 nJ. Following the absorption of the pump pulse, the thermo-elastic coupling leads to the generation of several acoustic waves over a broad spectral range from approximately 100 MHz to 100 GHz [20]. Notably, a longitudinal acoustic wave is launched in the *z*-direction. Due to the acoustic impedance mismatch at the W-Si interface, this wave bounces back and forth in the thin film and gives rise to acoustic echoes at the tungsten free surface. These echoes are detected by the probe pulse through the photoelastic interaction over the optical penetration depth in tungsten. The energy of the probe pulse at the sample position is 0.1 nJ. Following the pump pulse absorption, the thermo-elastic coupling leads also to the generation of GHz surface acoustic waves (SAWs) propagating in the *xy*-plane. The GHz frequency content of the SAWs is imposed by the lateral size ($\approx 1.5\mu$m) of the focus pump spot on the free surface of the film. The *xy* in-plane derivative of the normal displacement of the surface film is detected through a deflectometry detection scheme [38–41]. Figure 5 shows a raw experimental transient reflectivity at the epicenter over the first 10 ns. Following the coincidence, high frequency acoustic echoes (spikes just after the coincidence) and low frequency surface acoustic waves (up to $\approx$ 1.5ns) are clearly visible, as well as a slow thermal diffusion background. The absolute magnitude of the acoustic signals (echoes and SAWs) ranges from a few $10^{-5}$ to a few $10^{-4}$. Data shown in Fig. 5 have been acquired in 10 s and result from the averaging of 5000 acquisitions, leading to a signal resolution of $3\times10^{-6}$. High repetition rate ASOPS system present the advantage of a low acquisition time at the expense of the frequency resolution [3]. We have opted for lower repetition in order to get a higher spectral resolution at the expense of the acquisition time. In the following, the emphasis will be put on how the combination of a picosecond temporal resolution and a 48 MHz-spectral resolution allows to dynamically image at the same time 100 GHz BAWs and low GHz SAWs. This broadband acoustic imaging will give a thorough understanding on the propagation of SAWs at the surface of a supported thin film.

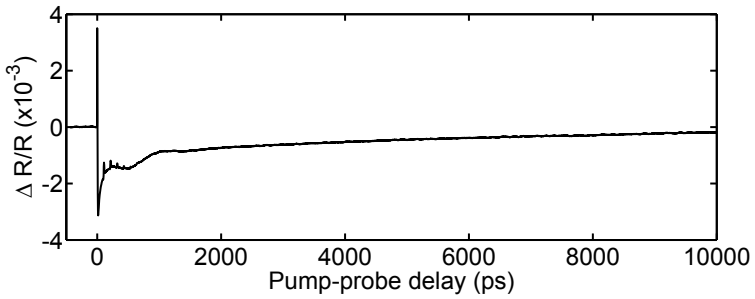


Fig. 5. Raw temporal signal at the epicenter over the first 10 ns. High frequency acoustic echoes as well as low frequency surface acoustic waves are clearly visible. The signal is only displayed up to 10 ns since acoustic features are located in the first nanoseconds after the coincidence.

### 3.3. Broadband opto-acoustic imaging

The acoustic echoes in the thin film contribute significatively to the transient reflectivity only a few microns away from the epicenter in the *xy* plane. Figure 6 shows $8\times8\,\mu$m$^2$ snapshots of the transient reflectivity centered on the epicenter and extracted at four pump-probe delays

#205233 - $15.00 USD Received 21 Jan 2014; revised 13 Mar 2014; accepted 16 Mar 2014; published 27 Mar 2014

$\tau$ (81 ps, 92 ps, 99 ps and 107 ps). The thermal diffusion background has been subtracted in the data presented in Fig. 6. The values of $\Delta R/R$, displayed on a color scale, directly bring information on the acoustic contribution. $\Delta R/R = 0$ corresponds to the red level. The spatially resolved acoustic echo is clearly visible with a $\Delta R/R$ minimum at $\tau = 92$ ps and maximum at $\tau = 99$ ps. These four snapshots demonstrate that dynamical imaging on a picosecond timescale can be achieved with the asynchronous pump-probe setup presented above.

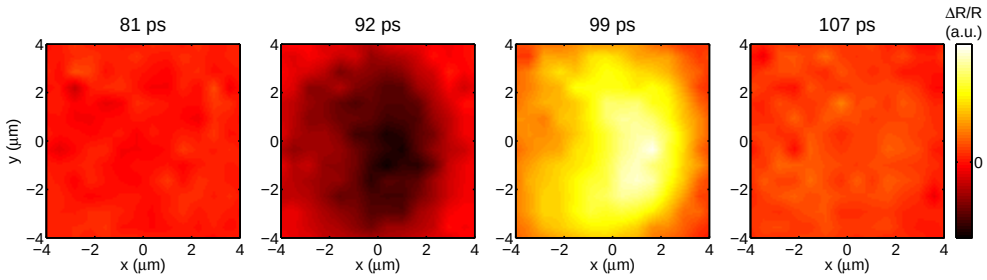


Fig. 6. Spatially resolved $\Delta R/R$ at four different pump-probe delays $\tau$ (81 ps, 92 ps, 99 ps and 107 ps) temporally centered on the first acoustic echoe. $\Delta R/R = 0$ corresponds to the red level.

While BAWs are confined close to the epicenter, SAWs propagate over tens of microns away from the opto-acoustic source location. Figure 7 shows $45 \times 45\,\mu\text{m}^2$ snapshots of the transient reflectivity extracted at four pump-probe delays $\tau$ (2900 ps, 5000 ps, 8000 ps and 14000 ps). Raw images consist of 300 pixels distributed over a $45\mu\text{m} \times 45\mu\text{m}$ surface. To obtain higher spatial resolution for the snapshots displayed in Fig. 7, we have taken benefit from the propagative feature of the acoustic waves. It implies that temporal and spatial scales are intrinsically related via the local instantaneous velocity of the acoustic waves. For each pixel at one given delay, a windowed time correlation between neighboring pixels allows to extract the group velocity as well as the propagation direction and thus to reconstruct the missing pixels. This approach is very robust to dispersion since we exploit the picosecond temporal resolution allowed by the ASOPS system (20,000 frames of 18x18 pixels over 20 ns). The velocity is thus recalculated for each pixel and each of the 20000 temporal steps. With this method, we can reach in each direction a 10-fold increase of the spatial resolution. $x$ and $y$ values denote the position relative to the epicenter. At such pump-probe delays and far away from the epicenter, the thermal contribution becomes negligible and the transient reflectivity, displayed on a color scale, carries information only on the acoustic contribution. $\Delta R/R = 0$ corresponds to the orange level. The signal in the upper-right corner of the snapshot at $\tau = 2900$ ps corresponds to SAWs generated by the previous pump pulse. At $\tau = 8000$ ps, two SAWs are clearly distinguished. The fastest SAW, in the upper-right corner of the snapshot, is almost not dispersive and is a surface skimming longitudinal wave (SSLW). The slowest and strongly dispersive SAW, as highlighted in the snapshot at $\tau = 14000$ ps, corresponds to a pseudo Rayleigh wave (PRW) [33, 42]. A more detailed analysis of the dispersion of the PRW will be carried out in section 3.5. Therefore, the 48 MHz-repetition rate of the lasers allows to retrieve information on the SAWs propagation over long temporal delays, or in other words with a high spectral resolution.

### *3.4. High frequency acoustic echoes - Determination of the thin film thickness*

Figure 8(a) shows the acoustic component of the transient reflectivity at the epicenter $(x = 0, y = 0)$ during the first hundreds of picoseconds after the excitation. The transient feature close

#205233 - $15.00 USD Received 21 Jan 2014; revised 13 Mar 2014; accepted 16 Mar 2014; published 27 Mar 2014

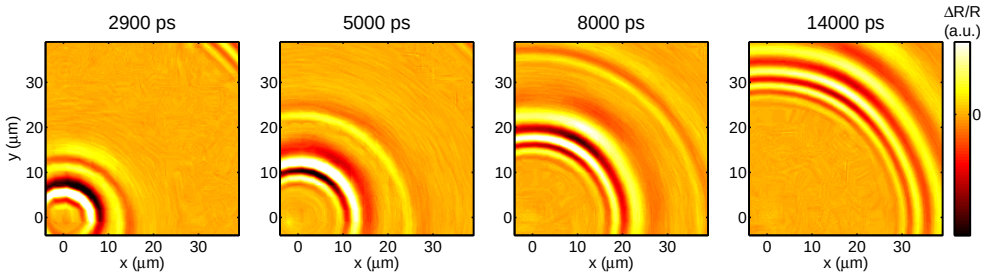


Fig. 7. Spatially resolved $\Delta R/R$, in arbitrary units, at four different pump-probe delays $\tau$ (2900 ps, 5000 ps, 8000 ps and 14000 ps). $\Delta R/R = 0$ corresponds to the orange level. Two SAWs are clearly distinguished on the snapshot at $\tau = 8000\,\text{ps}$.

to $\tau = 100\,\text{ps}$ is the acoustic echo resulting from the first round-trip of the high frequency BAW inside the thin film. The spatially resolved transient reflectivity of this echo has been presented in Fig. 6. Following this first echo, similar transient features with decreasing amplitude are detected at regular time intervals and correspond to several round-trips of the BAW inside the thin film. We assume bulk elastic parameters for the tungsten film [43]: $c_{11} = 523\,\text{GPa}$ and $c_{44} = 161\,\text{GPa}$. A film thickness $e = 252\,\text{nm}$ is thus deduced from the temporal delay $\Delta t = 97\,\text{ps}$ between two successive echoes. Figure 8(b) shows the spectrum of the transient reflectivity over the first hundreds of picoseconds displayed in Fig. 8(a) and illustrate that the frequency content of the detected acoustic echoes extends up to $\approx 150\,\text{GHz}$.

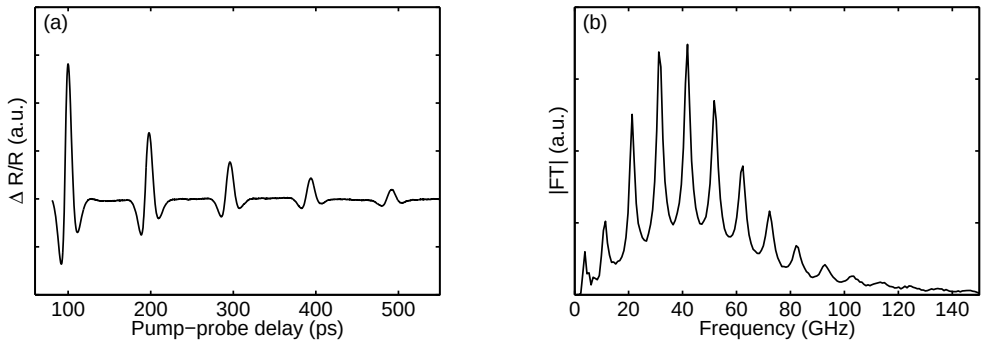


Fig. 8. (a) Acoustic signature of the high frequency bulk acoustic wave inside the thin film on the transient reflectivity $\Delta R/R$. The transient signals occurring at regular time intervals correspond to acoustic echoes detected at the free surface of the thin film. The temporal resolution is equal to 1 ps. (b) Spectrum of the transient reflectivity presented in panel (a) exhibiting a broad spectral content up to $\approx 150\,\text{GHz}$. The spectral resolution is equal to 48 MHz.

### *3.5. Low frequency surface acoustic waves - Analysis of the SAWs dispersion*

Despite acoustic anisotropy of silicon, acoustic wavefronts of the SAWs presented in Fig. 7 are almost perfectly circular in the *xy*-plane. This observation differs from results reported on SAWs propagating on a silicon substrate covered with a 50 nm thick gold film [32]. However, in the present case, the tungsten film is five time thicker and make the SAWs almost insensitive

#205233 - $15.00 USD Received 21 Jan 2014; revised 13 Mar 2014; accepted 16 Mar 2014; published 27 Mar 2014

to the acoustic anisotropy of silicon. Therefore, in the following, the SAWs propagation will be analyzed along one radius from the epicenter. The chosen radius is defined by $y = 0$ and $x > 0$. Figure 9 shows the dynamics of the transient reflectivity over 19 ns for 14 distances from the epicenter ranging from 2.8 to 38.4 $\mu$m. Continuous black curves correspond to experimental data. All the curves have been vertically upshifted for the sake of clarity. These results exhibit two distinct SAWs, the slower being strongly dispersive.

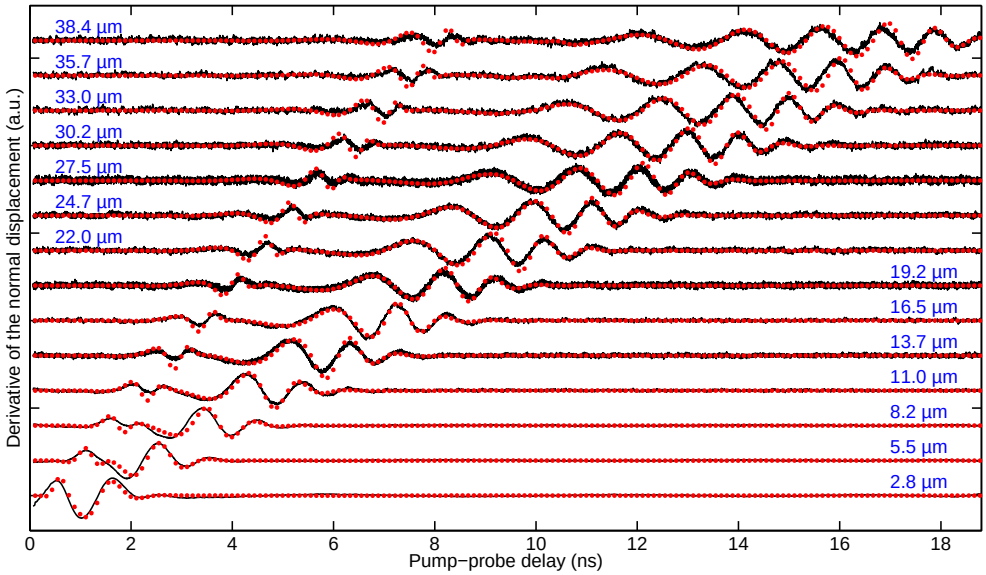


Fig. 9. Dynamics of the *xy* in-plane derivatives of the normal displacement of the surface film for 14 pump-probe distances. The value of each pump-probe distance is indicated in blue above each curve. Continuous black curves (resp. red dotted curves) correspond to experimental (resp. calculated) normalized signals. All curves have been vertically upshifted for the sake of clarity. The fastest SAW is a surface skimming longitudinal wave (SSLW) and the slowest and strongly dispersive SAW is a pseudo Rayleigh wave (PRW).

To identify more precisely these two waves, a semi-analytical calculation has been carried out. The underlying model describes the thermo-elastic generation of both volume and surface acoustic waves by a point source located at the free surface of a supported thin film [44, 45]. The calculated deflectometric signal, i.e. dynamics of the *xy* in-plane derivatives of the normal displacement of the surface film [38–41], are plotted in Fig. 9 as dotted red curves for the 14 pump-probe distances experimentally studied. Bulk elastic parameters have been assumed for the tungsten and for the silicon. It is important to emphasize that the thickness of the tungsten film has been chosen as the thickness $e = 252$ nm experimentally deduced from the time-of-flight of the high frequency acoustic echoes. The magnitudes of both experimental and simulated results have been normalized. Having in mind that the same set of elastic parameters has been used in the calculations for every pump-probe distance, the agreement between experimental and calculated results is excellent. In particular, the celerity of both the SSLW and the PRW as well as the strong dispersion of the latter are perfectly reproduced by the simulations and are in agreement with results previously reported [42].

To emphasize the 48 MHz-spectral resolution of the asynchronous dual-oscillator system, the group velocity dispersion of the PRW has been analyzed in the spectral domain. For each pump-probe distance $z_i$ ($i = 1..14$) considered in Fig. 9, the group velocity of the PRW $v_{g,i}(f)$, where $f$

#205233 - $15.00 USD Received 21 Jan 2014; revised 13 Mar 2014; accepted 16 Mar 2014; published 27 Mar 2014

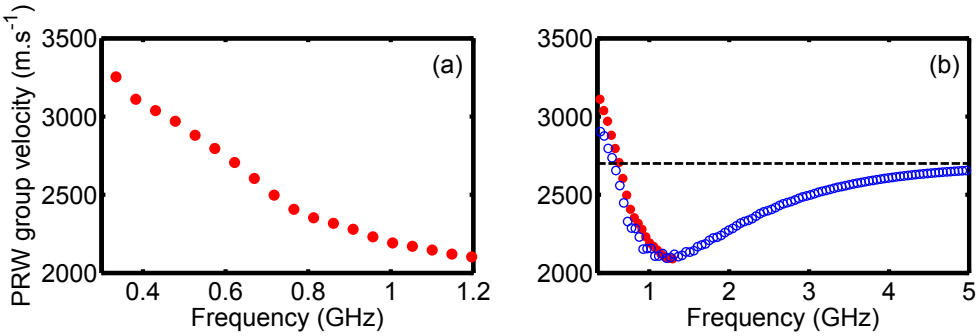


Fig. 10. (a) Experimentally deduced group velocity dispersion of the PRW. (b) Experimental (red dots, same data than in panel (a)) and calculated (blue open circles) dispersion of the group velocity of the PRW. A minimum in the group velocity is clearly visible close to 1.2 GHz. Dashed line: Rayleigh wave velocity at the free surface of a tungsten half-space.

is the frequency, has been extracted from the spectral phase $\phi_i(f)$ of the Fourier transform of the experimental temporal response : $v_{g,i}(f) = 2\pi z_i/(d\phi_i/df)$. The dispersion of $v_{g,i}$ is intrinsic to the geometry of the sample and does not depend on $z_i$. Figure 10(a) shows thus the frequency dependence of the group velocity dispersion averaged over the 14 pump-probe distances. A monotonic decrease of the group velocity with increasing frequency is observed. Nevertheless, the dispersion relation of the group velocity of a supported thin film is non-monotonic with respect to the frequency [46,47]. We do not experimentally observe this non-monotonic evolution since the frequency content of the detected PRW only extends up to 1.2 GHz: It is imposed by the lateral size ($\approx 1.5\mu$m) of the focus pump spot on the free surface of the film, as explained in section 3.2. To confirm this particular behavior, we have thus calculated the derivative of the normal displacement for a lateral spot size of the opto-acoustic source reduced down to 200 nm in order to broaden the spectral content of the PRW up to 5 GHz. We have extracted the group velocity dispersion by using the formula given above. Figure 10(b) shows the evolution of the experimental group velocity (red dots) already plotted in Fig. 10(a) as well as of the calculated (blue open circles) group velocity with respect to the frequency. A minimum in the calculated group velocity is clearly visible close to 1.2 GHz and the limit at high frequencies tends towards the Rayleigh velocity in a tungsten half-space [dashed line in Fig. 10(b)]. Furthermore, experimental and calculated dispersions are in strong agreement concerning this spectral behavior as well as on the values of the velocities. Concerning the low frequency part of the spectrum, the calculated group velocity at 0.3 GHz is close to $3000\,\mathrm{m.s}^{-1}$, i.e. well below the Rayleigh wave velocity at the free surface of a silicon half-space ($\approx 5100\,\mathrm{m.s}^{-1}$). Lower frequencies must be detected to reveal the silicon anisotropy. This observation is in agreement with the almost perfectly circular acoustic wavefronts in Fig. 7. It is important to emphasize that the identification of the acoustic group velocity dispersion in the thin film is only possible by using low repetition rates lasers (48 MHz) to get a very high spectral resolution.

## 4. Conclusion

In conclusion, we have presented an ASOPS-based picosecond ultrasonics setup with 48 MHz repetition rates. The relative timing jitter has been quantified and is of the order of or lower than 500 fs over the whole pump-probe delays. This asynchronous dual-oscillator system offers thus at the same time a picosecond temporal resolution and a 48 MHz spectral resolution. The acoustic response of a supported thin film excited by an opto-acoustic point source has been

#205233 - $15.00 USD Received 21 Jan 2014; revised 13 Mar 2014; accepted 16 Mar 2014; published 27 Mar 2014

investigated. Owing to the high temporal and high spectral resolutions of the ASOPS system high frequency acoustic echoes (up to 150 GHz) as well as low GHz SSLW and PRW could be imaged and group velocity dispersion of the PRW could be measured. A broadband opto-acoustic imaging is therefore performed over more than two decades. The determination of the thin film thickness from the time-of-flight of the acoustic echoes combined with semi-analytical calculations perfectly reproduce the velocity of both SAWs and the strong dispersion of the PRW. The 48 MHz spectral sampling has permitted to experimentally extract the group velocity dispersion of the PRW from 0.3 to 1.2 GHz. Experimentally deduced and calculated dispersion are in strong agreement. Due to its picosecond temporal resolution, the ASOPS pump-probe setup presented here should allow to perform broadband opto-acoustic imaging up to 500 GHz with a 48 MHz spectral resolution.

**Acknowledgments**

This work was financially supported by the Agence Nationale de la Recherche in France (project NanoVibe ANR11 JS09-013-01 and project Phemto), by the competitiveness cluster Route des Lasers and by the Région Aquitaine (project R09036GG).

#205233 - $15.00 USD Received 21 Jan 2014; revised 13 Mar 2014; accepted 16 Mar 2014; published 27 Mar 2014